J Mater Sci (2016) 51:6166–6172

A facile method for the production of SnS thin films from melt reactions

Mundher Al-Shakban[1], Zhiqiang Xie[1], Nicky Savjani[2], M. Azad Malik[1], and Paul O'Brien[1,2,*]

[1] School of Materials, University of Manchester, Oxford Road, Manchester M13 9PL, UK
[2] School of Chemistry, University of Manchester, Oxford Road, Manchester M13 9PL, UK

Received: 29 January 2016
Accepted: 16 March 2016
Published online: 8 April 2016

ABSTRACT

Tin(II)*O*-ethylxanthate [$Sn(S_2COEt)_2$] was prepared and used as a single-source precursor for the deposition of SnS thin films by a melt method. Polycrystalline, (111)-orientated, orthorhombic SnS films with controllable elemental stoichiometries (of between $Sn_{1.3}S$ and SnS) were reliably produced by selecting heating temperatures between 200 and 400 °C. The direct optical band gaps of the SnS films ranged from 1.26 to 1.88 eV and were strongly influenced by its Sn/S ratio. The precursor [$Sn(S_2COEt)_2$] was characterized by thermogravimetric analysis and attenuated total reflection Fourier-transform infrared spectroscopy. The as-prepared SnS films were characterized by scanning electron microscopy, energy-dispersive X-ray spectroscopy, powder X-ray diffractometry, Raman spectroscopy, and UV–Vis spectroscopy.

Introduction

Tin sulfides (SnS_2, Sn_2S_3, and SnS) are members of the IV–VI family of semiconductors that have shown promise in photovoltaic and optoelectronic applications [1–4]. Tin(II) sulfide (SnS) in particular has been seen as a potential candidate as an absorber layer in photovoltaic cells due to its 1.4 eV direct band gap that can harvest the visible and near-IR regions of the EM spectrum, the lower costs and toxicity of the constituent elements as compared to other potential materials (e.g., PbS and CdS), and the simplicity of the binary system compared to multicomponent materials such as copper zinc tin sulfide (CZTS) and copper indium gallium sulfide (CIGS) [5–8].

Single-source precursors (SSPs) are compounds that are designed to decompose to materials of specific compositions, by containing the desired elements. In many cases, the uses of SSPs have granted control of both its physical and optical properties that dual-source precursors cannot [9–11]. In the last 20 years [12–18], many SSPs comprised metal (*N*,*N*-dialkyldithiocarbamates) [$M(S_2CNR_2)_n$] have been used to synthesize metal sulfide nanocrystals. More recently, complexes containing (*O*-alkyl)xanthate ($^{-}S_2COAk$) ligands have been viewed as a potentially useful class of SSPs for the production of metal sulfide nanomaterials. The decomposition of metallo-organic xanthates is known to take place via the relatively low-temperature and clean Chugaev elimination reaction [19]. The use of the xanthate ligand in SSPs has

Address correspondence to E-mail: Paul.O'Brien@manchester.ac.uk

permitted the formation of many metal sulfides, including, but not limited to, MoS_2 [20], CdS [21], NiS, PdS [22], and CZTS [23], at lower temperatures than those needed by their respective (*N*,*N*-dialklydithiocarbamato-) analogs. Recently, we have reported the preparations of PbS/polymer composites from both lead(II)xanthate and lead(II)dithiocarbamate complexes by a melt process [18, 24], finding that the decomposition of $Pb(S_2CO^nBu)_2$ in a polymer matrix produced pure cubic PbS nanocrystals at 150 °C; significantly lower temperatures than 275 °C are needed to decompose $Pb(S_2CN^nBu_2)_2$. As a result, the xanthate-containing SSP can be used in a wider temperature window, giving greater control over nanocrystal size, shape variation, and orientation preference of the PbS crystals. Among the other known methods to SnS nanomaterials [18, 25], explorations of the syntheses of orthorhombic SnS nanoparticles [26–28] and films [13, 29, 30], using Sn-SSPs such as $[Sn^{II}(S_2CNR_2)_2]$ and $[R'_2Sn^{IV}(S_2CNR_2)_2]$, have been reported. To date, however, no studies on the uses of tin(*O*-alkylxanthate) complexes have been documented.

In this report, we investigate the use of the SSP $[Sn(S_2COEt)_2]$ as a coating material for the production of herzenbergite SnS films on glass. We focus on both the annealing temperature and the role of the xanthate ligand during the decomposition process for the potential in controlling the structural and optoelectronic properties of the SnS films produced.

Experimental

Materials and methods

Potassium ethyl xanthate, chloroform and tetrahydrofuran were purchased from Sigma-Aldrich. Tin(II) chloride was purchased from Alfa Aesar. All chemicals were used as received. Elemental (EA) and thermogravimetric (TGA) analyses were carried out by the Microelemental Analysis service at University of Manchester. EA was performed using a Flash 2000 Thermo Scientific elemental analyzer and TGA data obtained with Mettler Toledo TGA/DSC1 star^e system between the ranges of 30–600 °C at a heating rate of 10 °C min^{-1} under nitrogen flow. Scanning electron microscopy (SEM) analysis was performed using a Philips XL30 FEG microscope, with energy-dispersive X-ray spectroscopy (EDX) data obtained using a DX4 instrument. Thin-film X-ray diffraction (XRD) analyses were carried out using an X-Pert diffractometer with a Cu-$K_{\alpha 1}$ source ($\lambda = 1.54059$ Å), the samples were scanned between 20° and 75°, the applied voltage was 40 kV, and the current was 30 mA. Raman spectra were measured using a Renishaw 1000 Micro-Raman System equipped with a 514 nm laser. UV–Vis measurements were made using a Shimadzu UV-1800 spectrophotometer.

Synthesis of tin(II)(*O*-ethylxanthate)

$[Sn(S_2COEt)_2]$ was prepared by a procedure that was modified for that described in literature [19, 31]. An aqueous solution of potassium ethylxanthate (10.0 g, 12.5 mmol) was added to a stirred solution of tin(II) chloride (5.9 g, 6.2 mmol) in distilled water (100 ml) and stirred for a further 30 min. The yellow precipitate produced was filtered by vacuum filtration, washed three times with water, and finally dried in a vacuum oven at room temperature for 2 h. Yield = 7.2 g (67 %). Melting point = 44–53 °C. Anal. Calcd for $[Sn(S_2COEt)_2]$: C, 19.98; H, 2.79; S, 35.45; Sn, 32.91 Found: C, 19.67; H, 2.74; S, 35.45; Sn, 32.17. FTIR data (cm^{-1}); 2986.8 (w), 2930.7 (w), 1457 (w), 1355 (w), 1195.6 (s), 1108.1(s), 1020.6 (s), 852.0(w), 801.3(w), 563.4 (w).

Preparation SnS thin films by spin coating and heating

Glass slides were cut to 20 mm × 15 mm, cleaned by sonication in acetone (twice) and water, and allowed to dry. Three cycles of coating was performed; in each cycle, 300 μL of a 3 M $[Sn(S_2COEt)_2]$ solution in THF was coated onto the glass slide by spin coating at 700 rpm for 60 s and allowed to dry. The resulting films were loaded into a glass tube for decomposition in a dry nitrogen environment. The tube was then heated in the furnace to the desired temperature (150–400 °C) at a rate of ~3 °C min^{-1} and held at that temperature for 60 min; after this time had elapsed, the furnace was turned off and the tube allowed to cool to room temperature.

Results and discussion

The tin xanthate precursor $[Sn(S_2COEt)_2]$ was synthesized by the literature procedure [19, 31] and elemental analyses confirming its purity. The yellow

powder is readily soluble in THF and many other common organic solvents. It was found that storage at −20 °C was necessary to limit decomposition. The thermal decomposition of $[Sn(S_2COEt)_2]$ was studied using thermogravimetric analysis (TGA). The thermogram showed rapid single decomposition step between 80 and 130 °C (Fig. S1). The final weight of the residue (44.1 %) is close to the predicted value for residual SnS (41.8 %). The precursor is predicted to break down via the Chugaev elimination mechanism [19], as shown in Scheme S1. The IR spectrum of $[Sn(S_2COEt)_2]$ shows bands corresponding to ν(C–O) (1196 and 1224 cm^{-1}) and ν(C–S) (1021 and 1108 cm^{-1}). A peak at 563 cm^{-1} is also observed consistent with a ν(Sn–S) mode (Fig. S2).

SnS films were prepared by coating glass slides with the $[Sn(S_2COEt)_2]$ precursor, followed by heating step in an N_2 environment, at 150, 200, 250, 300 and 400 °C for 1 h. The resulting films were gray and uniform at all the heating temperatures (Fig. S3); the films were found to be between 2.2 and 2.9 μm thick. Both the morphology and composition of the SnS films produced showed a dependence on the heating temperature. The films contained nearly spherical structures with some flakes (Fig. 1a, b, c, d). Elemental maps for the film produced at all temperatures (elemental maps for 300 °C shown in Fig. 1e, f; maps for the other films in Fig. S4) demonstrate the uniform distribution of these elements among the films. The Sn/S ratio within the films steadily decreased when higher reaction temperatures were used (Table 1; Fig. 2): Sn/S ratios of 1.31 and 1.32 ($Sn_{1.31}S$ and $Sn_{1.32}S$) were seen in the films produced at 150 and 200 °C (sulfur deficient). Increasing the heating temperature also increased the sulfur content in the film, reactions performed at 250 and 300 °C produced SnS films with reduced sulfur deficiency (Sn/S ratios of 1.15:1 ($Sn_{1.15}S$) and 1.11:1 ($Sn_{1.11}S$), respectively), and a stoichiometric SnS film was obtained upon heating at 400 °C (Sn/S ratio 1.03:1; ($Sn_{1.03}S$)). Such control of the stoichiometry in SnS nanomaterials has previously been observed [32, 33].

The p-XRD patterns of the SnS thin films produced at temperatures between 200 and 400 °C gave peaks that can be indexed to herzenbergite-SnS with the expected orthorhombic crystal structure (matches ICCD pattern No. 00-039-0354; see Fig. 3a); no other peaks are observed that correspond to other tin oxide or sulfide species. The calculated unit cell parameters of the herzenbergite SnS films (shown in Table 1) match the expected (Pbnm) space group, with lattice parameters that closely match with those reported in literature [34, 35]. The films heated at 400 °C have strong, well-defined diffraction peaks. At lower temperatures, however, the films were found to exhibit broader peaks, possibly due to the increasing sulfur deficiency within the crystalline film. The temperature during $[Sn(S_2COEt)_2]$ decomposition seems crucial; at lower temperatures, the rate at which the precursor decomposes will be slowed

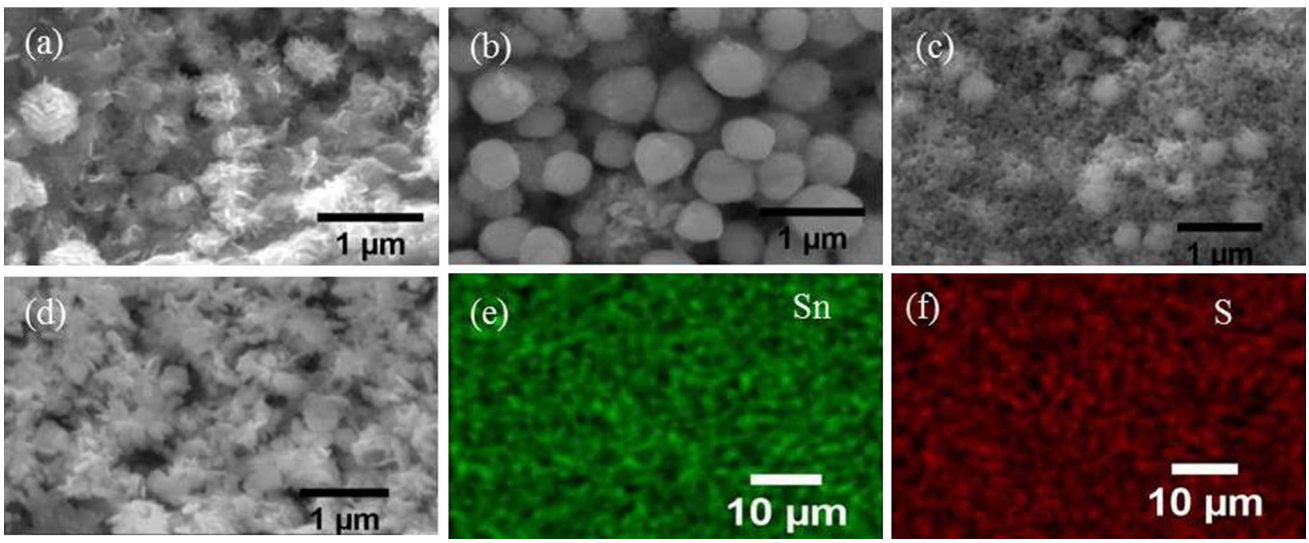

Figure 1 SEM images of SnS films grown on glass substrates from $[Sn(S_2COEt)_2]$ at **a** 200 °C, **b** 250 °C, **c** 300 °C, and **d** 400 °C (*scale bars* represent 1 μm); **e** and **f** the elemental maps of the SnS film produced at 300 °C (*scale bars* represent 10 μm).

Table 1 Thicknesses, compositions, and unit cell parameters of the SnS films produced by the melt method

Heating Temp. (°C)	Thickness (μm)	Sn atomic (%)[a]	S atomic (%)[a]	Sn/S ratio	Unit cell parameters (orthorhombic, Å)[b,c]
150	–	56.8	43.2	1.31:1 (± 0.07)	$a = 4.355$, $b = 11.232$, $c = 3.985$
200	2.2	56.99	43.0	1.32:1 (± 0.07)	$a = 4.324$, $b = 11.237$, $c = 3.980$
250	2.9	53.4	46.4	1.15:1 (± 0.06)	$a = 4.324$, $b = 11.231$, $c = 3.984$
300	2.8	52.5	47.5	1.11:1 (± 0.06)	$a = 4.324$, $b = 11.236$, $c = 3.986$
400	2.5	50.7	49.3	1.03:1 (± 0.05)	$a = 4.324$, $b = 11.219$, $c = 3.986$

[a] Determined by SEM–EDX

[b] Determined by p-XRD

[c] Rock-salt SnS phase also observed in the films produced at 150 °C (unit cell parameter: $a = 5.801$ Å)

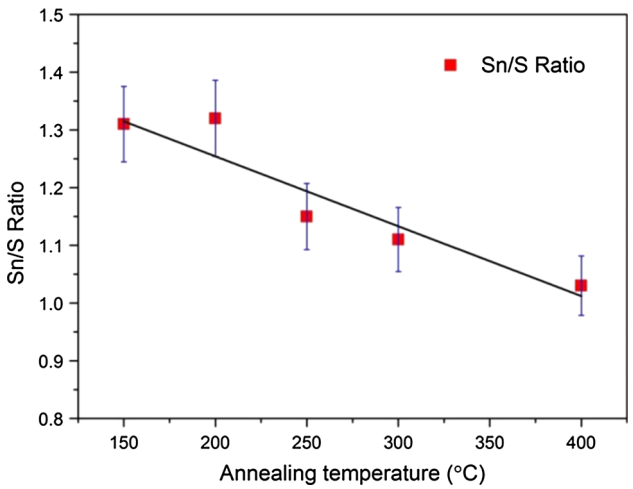

Figure 2 The Sn/S ratio by EDX for samples heated for 60 min at temperatures between 150 and 400 °C.

considerably, with the resulting intermediate species exposed to temperatures that may promote evaporation. In contrast, the $Sn_{1.31}S$ film produced at 150 °C was found to consist of a mixture of orthorhombic and cubic phases, with the latter phase matching well with a rock-salt SnS phase (space group Fm-3 m; ICCD pattern No. 04-004-8426) recently discussed by first-principle calculations [36, 37]. In addition, Raman spectroscopy of all of the SnS films (Fig. 3b) revealed Raman bands at 94, 160, 188, and 218 cm^{-1}, in good agreement with the herzenbergite SnS phase reported previously [38–40].

The optical band gaps (E_g) of the SnS films (produced at temperatures between 200 and 400 °C) were determined from optical absorption measurements by the Tauc method (Fig. 4a) [41, 42]. All of the films analyzed have high absorption coefficients ($\alpha > 10^4$ cm^{-1} above the fundamental absorption). The band gaps were evaluated by extending linear part of the plots of $(\alpha hv)^2$ versus hv [43]. The band gap of the $Sn_{1.32}S$ films formed at 200 °C is 1.88 eV. Increased decomposition temperatures gave lower band gaps; 250 ($Sn_{1.15}S$), 300 ($Sn_{1.11}S$), and 400 °C ($Sn_{1.03}S$) gave band gaps at 1.75, 1.49, and 1.26 eV, respectively. It is clear that the control of the stoichiometry that we have achieved in the syntheses allows for tuning of optical band gaps. The band gaps of SnS films previously reported [44–48] show similar change with sulfur deficiency (Fig. 4b). However, care needs to be taken when comparing the results obtained from literature to our dataset, as the films produced by each citation varies from both our work and each other. These experimental variations will introduce variations in the macrostructures, elemental stoichiometries, film thicknesses, and concentrations of Sn_xS_y-based impurities contained within the SnS films documented. The physical properties of the materials and the potential of quantum confined materials may also need to be considered.

Conclusions

A simple process has been described for the growth of SnS films. Heating of substrates spin-coated with tin(II)*O*-ethylxanthate at different temperatures between 150 and 400 °C produced SnS films mainly in orthorhombic phase with good crystallinity. Analyses of the films reveal them to be sulfur deficient with Sn/S ratio controlled by selecting the heating temperatures. In addition, a correlation was found between the optical band gap of the SnS films (as determined by UV–Vis spectroscopy) and the stoichiometry. The measured optical band gaps were lowered from 1.88 to 1.26 eV. We believe that the

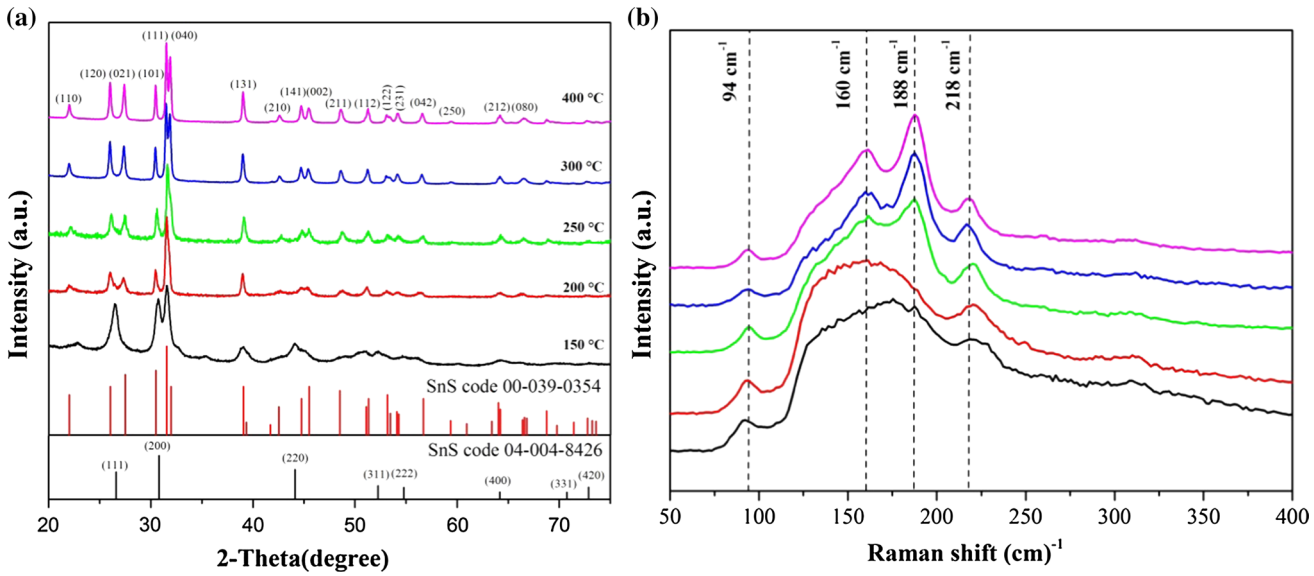

Figure 3 **a** p-XRD patterns of SnS films grown on glass substrate at different temperatures, accompanied by reference patterns of herzenbergite SnS (ICCD pattern No. 00-039-0354) and rock-salt SnS (ICCD pattern No. 04-004-8426). **b** Raman spectra for the SnS films grown on glass substrates from $[Sn(S_2COEt)_2]$ at 150, 200, 250, 300, and 400 °C.

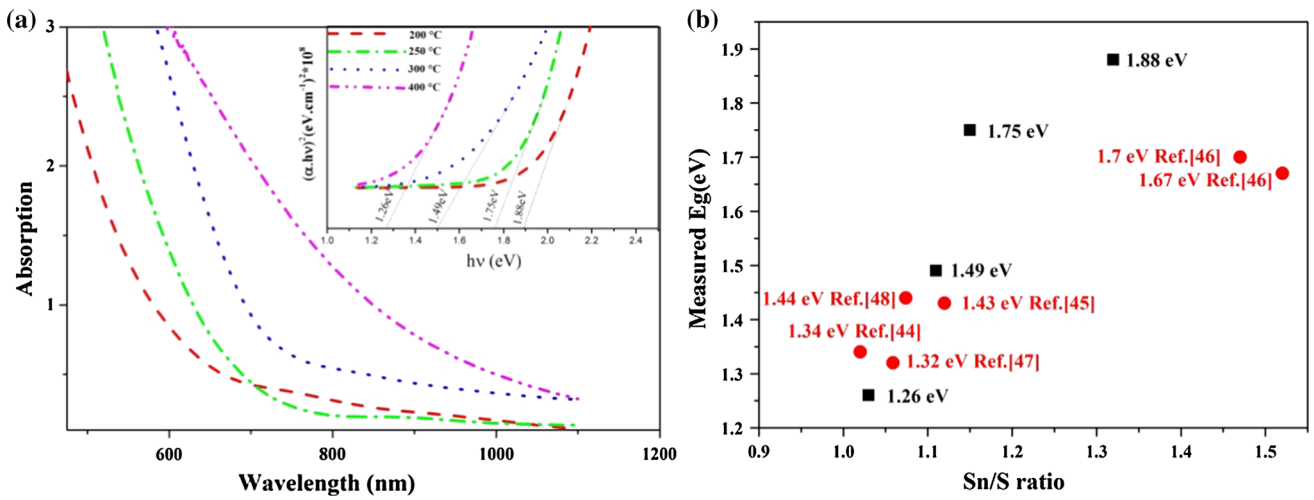

Figure 4 **a** UV–Vis and Tauc plots (*inset*) for the SnS films grown on glass substrates from $[Sn(S_2COEt)_2]$ at 200, 250, 300, and 400 °C. **b** Graph showing the relationship between the Sn/S ratio of SnS_{1-x} materials with its measured band gap. Data in *black* represents the findings in this report, whereas data in *red* were obtained from literature.

process described in this report could be used in the production of SnS films with tuneable band gaps for solar cell applications.

Acknowledgements

The authors would like to acknowledge the EPSRC Core Capability in Chemistry (CCC), Grant Number EP/K039547/1 (Director: Prof. Gareth Morris), for access to numerous analytical equipment. The authors would also like to thank Dr. Christopher Wilkins at School of Materials University of Manchester for helpful discussions on SEM and EDX. MAS acknowledges the Iraqi Culture Attaché in London for financial support. NS thanks the Parker family for funding his position.

Compliance with ethical standards

Conflict of Interest The authors declare that they have no conflict of interest.

Electronic supplementary material: The online version of this article (doi:10.1007/s10853-016-9906-7) contains supplementary material, which is available to authorized users.

References

[1] Reddy KTR, Reddy NK, Miles RW (2006) Photovoltaic properties of SnS based solar cells. Sol Energ Mater Sol Cells 90:3041–3046

[2] Lei Y, Song S, Fan W, Xing Y, Zhang H (2009) Facile synthesis and assemblies of flowerlike SnS_2 and In^{3+}-doped SnS_2: hierarchical structures and their enhanced photocatalytic property. J Phys Chem C 113:1280–1285

[3] Motevalizadeh L, Khorshidifar M, Abrishami ME, Moghagheghi MMB (2013) Nanocrystalline ITO-Sn_2S_3 transparent thin films for photoconductive sensor applications. J Mater Sci 24:3694–3700

[4] Zhu H, Yang D, Ji Y, Zhang H, Shen X (2005) Two-dimensional SnS nanosheets fabricated by a novel hydrothermal method. J Mater Sci 40:591–595. doi:10.1007/s10853-005-6293-x

[5] Ichimura M (2009) Calculation of band offsets at the CdS/SnS heterojunction. Sol Energy Mater Sol Cells 93:375–378

[6] Ghosh B, Das M, Banerjee P, Das S (2009) Fabrication of the SnS/ZnO heterojunction for PV applications using electrodeposited ZnO films. Semicond Sci Technol 24:025024

[7] Dussan A, Mesa F, Gordillo G (2010) Effect of substitution of Sn for Bi on structural and electrical transport properties of SnS thin films. J Mater Sci 45:2403. doi:10.1007/s10853-010-4207-z

[8] Robles V, Trigo JF, Guillén C, Herrero J (2013) Structural, chemical, and optical properties of tin sulfide thin films as controlled by the growth temperature during co-evaporation and subsequent annealing. J Mater Sci 48:3943–3949. doi:10.1007/s10853-013-7198-8

[9] Lazell M, O'Brien P, Otway D, Park J-H (2000) Single source molecular precursors for the deposition of III/VI chalcogenide semiconductors by MOCVD and related techniques. J Chem Soc Dalton Trans 24:4479–4486

[10] Castro SL, Bailey SG, Raffaelle RP, Banger KK, Hepp AF (2004) Synthesis and characterization of colloidal $CuInS_2$ nanoparticles from a molecular single-source precursor. J Phys Chem 108:12429–12435

[11] Tian L, Tan HY, Vittal JJ (2007) Morphology-controlled synthesis of Bi_2S_3 nanomaterials via single-and multiple-source approaches. Cryst Growth Des 8:734–738

[12] Trindade T, O'Brien P, Zhang X-M (1997) Synthesis of CdS and CdSe nanocrystallites using a novel single-molecule precursors approach. Chem Mater 9:523–530

[13] Kevin P, Lewis DJ, Raftery J, Malik MA, O'Brien P (2015) Thin films of tin(II) sulphide (SnS) by aerosol-assisted chemical vapour deposition (AACVD) using tin(II) dithiocarbamates as single-source precursors. J Cryst Growth 415:93–99

[14] Trindade T, O'Brien P, Pickett NL (2001) Nanocrystalline semiconductors: synthesis, properties, and perspectives. Chem Mater 13:3843–3858

[15] O'Brien P, Nomura R (1995) Single-molecule precursor chemistry for the deposition of chalcogenide (S or Se) containing compound semiconductors by MOCVD and related methods. J Mater Chem 5:1761–1773

[16] Malik MA, Afzaal M, O'Brien P (2010) Precursor chemistry for main group elements in semiconducting materials. Chem Rev 110:4417–4446

[17] Ramasamy K, Malik MA, Revaprasadu N, O'Brien P (2013) Routes to nanostructured inorganic materials with potential for solar energy applications. Chem Mater 25:3551–3569

[18] Lewis DJ, Kevin P, Bakr O, Muryn CA, Malik MA, O'Brien P (2014) Routes to tin chalcogenide materials as thin films or nanoparticles: a potentially important class of semiconductor for sustainable solar energy conversion. Inorg Chem Front 1:577–598

[19] Kociok-Köhn G, Molloy KC, Sudlow AL (2014) Molecular routes to Cu_2ZnSnS_4: a comparison of approaches to bulk and thin film materials. Can J Chem 92:514–524

[20] Savjani N, Brent JR, O'Brien P (2015) AACVD of molybdenum sulfide and oxide thin films from molybdenum (V) based single-source precursors. Chem Vap Depos 21:71–77

[21] Pradhan N, Efrima S (2003) Single-precursor, one-pot versatile synthesis under near ambient conditions of tunable, single and dual band fluorescing metal sulfide nanoparticles. J Am Chem Soc 125:2050–2051

[22] Cheon J, Talaga DS, Zink JI (1997) Laser and thermal vapor deposition of metal sulfide (NiS, PdS) films and in situ gas-phase luminescence of photofragments from $M(S_2COCHMe_2)_2$. Chem Mater 9:1208–1212

[23] Fischereder A, Schenk A, Rath T, Haas W, Delbos S, Gougaud C, Naghavi N, Pateter A, Saf R, Schenk D (2013)

Solution-processed copper zinc tin sulfide thin films from metal xanthate precursors. Monatsh Chem 144:273–283

[24] Lewis EA, Mcnaughter PD, Yin Z, Chen Y, Brent JR, Saah SA, Raftery J, Awudza JAM, Malik MA, O'Brien P, Haigh S (2015) In situ synthesis of PbS nanocrystals in polymer thin films from lead(II) xanthate and dithiocarbamate complexes: evidence for size and morphology control. Chem Mater 27:2127–2136

[25] Brent JR, Lewis DJ, Lorenz T, Lewis EA, Savjani N, Haigh SJ, Seifert G, Derby B, O'Brien P (2015) Tin(II) sulfide (SnS) nanosheets by liquid-phase exfoliation of herzenbergite: IV–VI main group two-dimensional atomic crystals. J Am Chem Soc 137:12689–12696

[26] Petkov N, Xu J, Morris MA, Holmes JD (2008) Confined growth and crystallography of one-dimensional Bi_2S_3, CdS, and SnS_x nanostructures within channeled substrates. J Phys Chem C 112:7345–7355

[27] Ning J, Men K, Xiao G, Wang L, Dai Q, Zou B, Liu B, Zou G (2010) Facile synthesis of IV–VI SnS nanocrystals with shape and size control: nanoparticles, nanoflowers and amorphous nanosheets. Nanoscale 2:1699–1703

[28] Hong SY, Popovitz-Biro R, Prior Y, Tenne R (2003) Synthesis of SnS_2/SnS fullerene-like nanoparticles: a superlattice with polyhedral shape. J Am Chem Soc 125:10470–10474

[29] Ramasamy K, Kuznetsov VL, Gopal K, Malik MA, Raftery J, Edwards PP, O'Brien P (2013) Organotin dithiocarbamates: single-source precursors for tin sulfide thin films by aerosol-assisted chemical vapor deposition (AACVD). Chem Mater 25:266–276

[30] Xu Z, Chen Y (2012) Fabrication of SnS thin films by a novel multilayer-based solid-state reaction method. Semicond Sci Technol 27:035007

[31] Raston C, Tennant PR, White AH, Winter G (1978) Reactions of tin(II) and tin(IV) xanthates: crystal structure of Tetrakis(O-ethylxanthato)tin(IV). Aust J Chem 31:1493–1500

[32] Robles V, Trigo JF, Guillén C, Herrero J (2015) SnS absorber thin films by co-evaporation: optimization of the growth rate and influence of the annealing. Thin Solid Films 582:249–252

[33] Ichimura M, Takeuchib K, Onob Y, Arai E (2000) Electrochemical deposition of SnS thin films. Thin Solid Films 361:98–101

[34] Wiedemeier H, Schnering HGV (1978) Refinement of the structures of GeS, GeSe, SnS and SnSe. Z Kristallogr 148:295–303

[35] El-Nahass MM, Zeyada HM, Aziz MS, El-Ghamaz NA (2002) Optical properties of thermally evaporated SnS thin films. Opt Mater 20:159–170

[36] Burton LA, Walsh A (2012) Phase stability of the earth-abundant tin sulfides SnS, SnS_2, and Sn_2S_3. J Phys Chem C 116:24262–24267

[37] Sun Y, Zhong Z, Shirakawa T, Franchini C, Li D, Li Y, Yunoki S, Chen X-Q (2013) Rock-salt SnS and SnSe: native topological crystalline insulators. Phys Rev B 88:235122

[38] Chandrasekhar HR, Humphreys RG, Zwick U, Cardona M (1977) Infrared and Raman spectra of the IV-VI compounds SnS and SnSe. Phys Rev B 15:2177

[39] Sinsermsuksakul P, Heo J, Noh W, Hock AS, Gordon RG (2011) Atomic layer deposition of tin monosulfide thin films. Adv Energy Mater 1:1116–1125

[40] Price LS, Parkin IP, Hardy AME, Clark RJH, Hibbert TG, Molloy KC (1999) Atmospheric pressure chemical vapor deposition of tin sulfides (SnS, Sn_2S_3, and SnS_2) on glass. Chem Mater 11:1792–1799

[41] Jain P, Arun P (2013) Influence of grain size on the band-gap of annealed SnS thin films. Thin Solid Films 548:241–246

[42] Koktysh DS, McBride JR, Rosenthal SJ (2007) Synthesis of SnS nanocrystals by the solvothermal decomposition of a single source precursor. Nanoscale Res Lett 2:144–148

[43] Tanuševski A, Poelman D (2003) Optical and photoconductive properties of SnS thin films prepared by electron beam evaporation. Sol Energy Mater Sol Cells 80:297–303

[44] Yue GH, Peng DL, Yan PX, Wang LS, Wang W, Luoa XH (2009) Structure and optical properties of SnS thin film prepared by pulse electrodeposition. J Alloys Compd 468:254–257

[45] Ghosh B, Das M, Banerjee P, Das S (2008) Fabrication and optical properties of SnS thin films by SILAR method. App Surf Sci 254:6436–6440

[46] Calixto-Rodriguez M, Martinez H, Sanchez-Juarez A, Campos-Alvarez J, Tiburcio-Silver A, Calixto ME (2009) Structural, optical, and electrical properties of tin sulfide thin films grown by spray pyrolysis. Thin Solid Films 517:2497–2499

[47] Reddy NK, Reddy KTR (1998) Growth of polycrystalline SnS films by spray pyrolysis. Thin Solid Films 325:4–6

[48] Xu Z, Chen Y (2011) Synthesis of SnS thin films from nano-multilayer technique. Energy Procedia 10:238–242